PAPER

A lithium–air battery and gas handling system demonstrator†

Jack W. Jordan, [ID] [ab] Ganesh Vailaya,[a] Conrad Holc, [ID] [a] Max Jenkins,[bc] Rory C. McNulty, [ID] [ab] Constantin Puscalau,[d] Begum Tokay, [ID] [d] Andrea Laybourn, [ID] [d] Xiangwen Gao,[c] Darren A. Walsh, [ID] [ab] Graham N. Newton, [ID] [ab] Peter G. Bruce [ID] [bc] and Lee R. Johnson [ID] *[ab]

The lithium–air (Li–air) battery offers one of the highest practical specific energy densities of any battery system at >400 W h kg_{system}^{-1}. The practical cell is expected to operate in air, which is flowed into the positive porous electrode where it forms Li_2O_2 on discharge and is released as O_2 on charge. The presence of CO_2 and H_2O in the gas stream leads to the formation of oxidatively robust side products, Li_2CO_3 and LiOH, respectively. Thus, a gas handling system is needed to control the flow and remove CO_2 and H_2O from the gas supply. Here we present the first example of an integrated Li–air battery with in-line gas handling, that allows control over the flow and composition of the gas supplied to a Li–air cell and simultaneous evaluation of the cell and scrubber performance. Our findings reveal that O_2 flow can drastically impact the capacity of cells and confirm the need for redox mediators. However, we show that current air–electrode designs translated from fuel cell technology are not suitable for Li–air cells as they result in the need for higher gas flow rates than required theoretically. This puts the scrubber under a high load and increases the requirements for solvent saturation and recapture. Our results clarify the challenges that must be addressed to realise a practical Li–air system and will provide vital insight for future modelling and cell development.

Introduction

The lithium–air (Li–air) battery has a theoretical material-level specific energy of 3500 W h kg^{-1}, making it a leading next-generation electrochemical energy storage technology for high-energy applications.[1–4] The Li–air battery exploits the two-electron reduction of O_2 at a porous, carbon positive electrode, forming Li_2O_2,

[a]*Nottingham Applied Materials and Interfaces Group, School of Chemistry, University of Nottingham, Nottingham, NG7 2TU, UK. E-mail: lee.johnson@nottingham.ac.uk*

[b]*The Faraday Institution, Harwell Campus, Didcot, OX11 0RA, UK*

[c]*Department of Materials, University of Oxford, Parks Road, Oxford, OX1 3PH, UK*

[d]*Faculty of Engineering, University of Nottingham, Nottingham, NG7 2RD, UK*

with the concomitant oxidation of Li metal at the negative electrode.[5] During charging, the reactions are reversed, reforming O_2 and Li. However, the battery faces significant challenges,[3,6,7] such as degradation of the electrolyte during operation,[8–12] slow electrochemistry due to the insulating nature of Li_2O_2,[13–15] resulting in the need for homogeneous redox mediators to oxidise Li_2O_2,[16–22] instability of Li metal[23] and the need for anode-protection layers.[24] Significant progress has been made in these areas, however, most studies of the Li–air battery involve the use of pure O_2 gas as the feedstock for the positive electrode and often only low-capacity systems (<1 mA h cm^{-2}) are explored. Some examples of more practical cell configurations, albeit without gas-handling systems, have been reported.[25] Kubo and co-workers described a multilayer pouch cell that could store 150 W h kg$_{cell}$$^{-1}$ at 0.5 mA h cm^{-2},[26] while Zhao and co-workers reported a double-layer pouch cell with a capacity of >750 W h kg$_{cell}$$^{-1}$.[27] More recently, Lee and co-workers demonstrated a 1200 W h kg$_{cell}$$^{-1}$ folded pouch cell configuration that greatly exceeds the specific energy density possible by most battery technologies.[28,29] Practical, "real-world" Li–air batteries will operate in air, exposing the electrolyte to H_2O and CO_2, which can react with Li_2O_2 to yield LiOH and Li_2CO_3 respectively.[30] LiOH can cause electrolyte degradation, and both salts have high oxidation potentials, which would significantly limit the coulombic efficiency of the cell.[31,32] Due to the challenges associated with atmospheric gases on the operation of Li–air cells, "real-world" open devices will incorporate gas-handling systems to "scrub" the air[33] of H_2O and CO_2 and it is assumed that concentrations of <10 ppm are needed for both.[34]

Gallagher *et al.* proposed theoretical system models for a practical air-breathing (open) battery comprising a gas-feed stream and an air scrubber system. The gas-handling system significantly impacted the system-level performance of the Li–air pack according to the BatPac model.[34] No experimental data on the requirements of a practical gas purification system have been reported. Some work has probed the effects of parameters such as gas composition,[35] O_2 partial pressure[36] and gas flow[37,38] on the capacity of Li–air cells, but usually in cells operating at unrealistically low current densities (<100 µA cm^{-2}) and large flow rates. Progress towards the development of a practical Li–air battery requires a holistic view of the challenges involved, including not only the chemical and electrochemical processes occurring within the cell, but also of the effects of the gas-handling parameters on device performance. Delivery of air and removal of CO_2 and H_2O from the input stream are inherently linked; efficient delivery of air to the cell will require higher flow rates, which will increase the workload of the scrubber system. Such effects must be considered in tandem during device testing to provide realistic estimates of cell performance.

Here we describe the first example of an integrated Li–air battery demonstrator with in-line gas handling system, consisting of the cell, atmospheric control and gas scrubber chamber. The cell is based on a fuel cell design and the gas handling system controls the flow and pressure of the gas to the cell. The cell incorporates a flow field to distribute the gas flow over the positive electrode. The impact of gas flow rate and composition is explored and we show that this has a drastic impact on cell performance. Our analysis highlights some deficiencies in the design of current flow field plates, gas diffusion electrodes, and gas scrubber materials when used in Li–air cells, thus highlighting where further innovation is needed if we are to achieve a practical air-breathing Li–air system.

Results and discussion

To evaluate the impact of gas composition, flow rates and scrubber material on the performance of the Li–air cell and gas handling system, we developed a demonstrator battery system (Fig. 1) in which the composition (including the humidity), pressure, and flow rate of the gas delivered to the cell can be controlled. The gas handling system was constructed from stainless steel Swagelok tubing and the cell was based on a fuel cell stack, which contains a technologically mature gas delivery design, albeit optimised for aqueous systems.[39] The three inlet gas compositions used were 100% O_2, 20% O_2 (balanced with N_2) and compressed air. The gas could either be routed through the scrubber or passed directly to the cell. The scrubber consisted of a steel tube (5 cm diameter, 15 cm length), which could be heated and placed under vacuum to regenerate the scrubber media. The scrubber volume far exceeded that of the cell, an unrealistic and best-case scenario for the practical system, and thus the limiting factor should be the performance of the materials used to remove H_2O and CO_2. Two in-
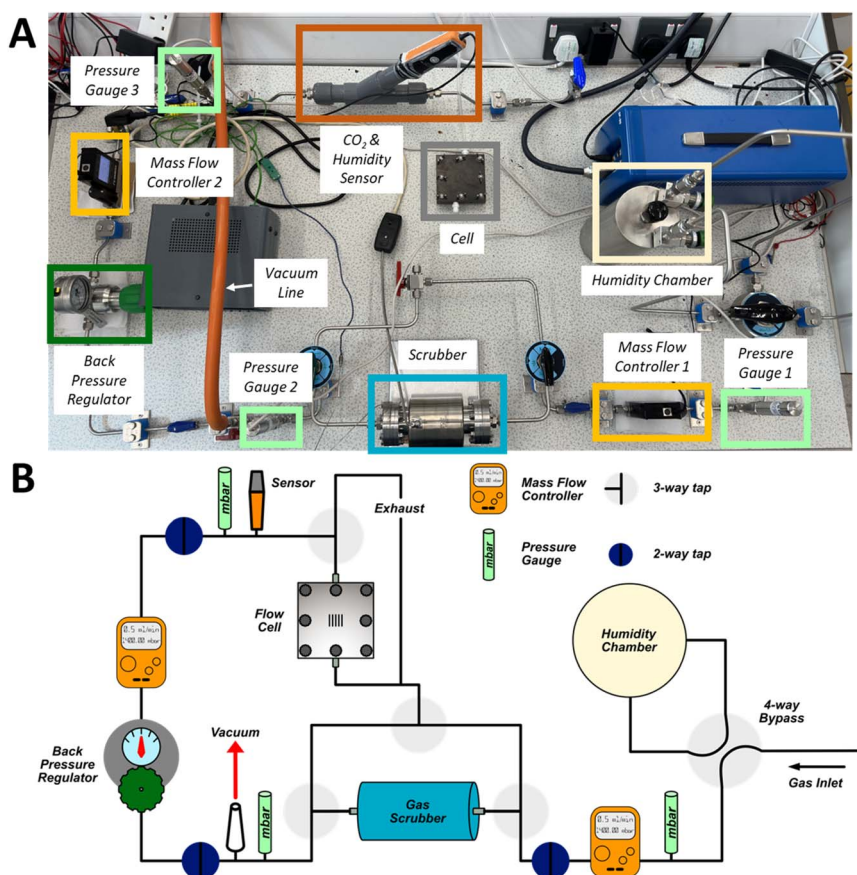

Fig. 1 (A) Photograph of the Li–air demonstrator system with labelled components. (B) A schematic diagram of the Li–air demonstrator system. A description of the design can be found in the text.

line mass flow controllers were used to control flow rates to the cell; one was positioned before the scrubber and one before the cell. A back-pressure regulator was positioned after the scrubber to compensate for the pressure drop as gas was routed through the scrubber. Pressure gauges placed at three locations allowed continuous monitoring of the system pressure. For all experiments, the gas inlet section was pressurised to about 1400 mbar, with a pressure of about 1000 mbar before the cell. A sensor measured the CO_2 content and humidity of the gas entering the cell.

The open cell (Fig. 2A and B) was composed of a graphite plate with serpentine-type flow field for gas delivery to the positive electrode, a steel plate current collector for the negative electrode, and a stainless-steel mesh current collector for the positive electrode. A polytetrafluoroethylene (PTFE) gasket was used to separate the two plates. As is typical in the field, freestanding pre-charged $LiFePO_4$ (LFP) was used as the negative electrode (350 μm thickness, 22 mm × 22 mm) rather than Li, as the latter requires the development of a protected Li anode to avoid reactions with the electrolyte. Free standing 20 × 20 mm Super P cathodes (80 : 20 wt% Super P : PTFE) were used as the positive electrode. A glass fibre separator was placed between the electrodes. The electrolyte for all experiments was 150 μL cm^{-2} of 1.0 M lithium bis(trifluoromethane)sulfonimide (LiTFSI) dissolved in tetraethylene glycol dimethyl ether (tetraglyme) unless otherwise stated.

Cells discharged at 0.5 mA cm^{-2} under a flowing excess of 100% O_2 (0.50 mL min^{-1}) yielded a relatively low capacity of 0.7 mA h cm^{-2} to a cut-off of 2.3 V $vs.$
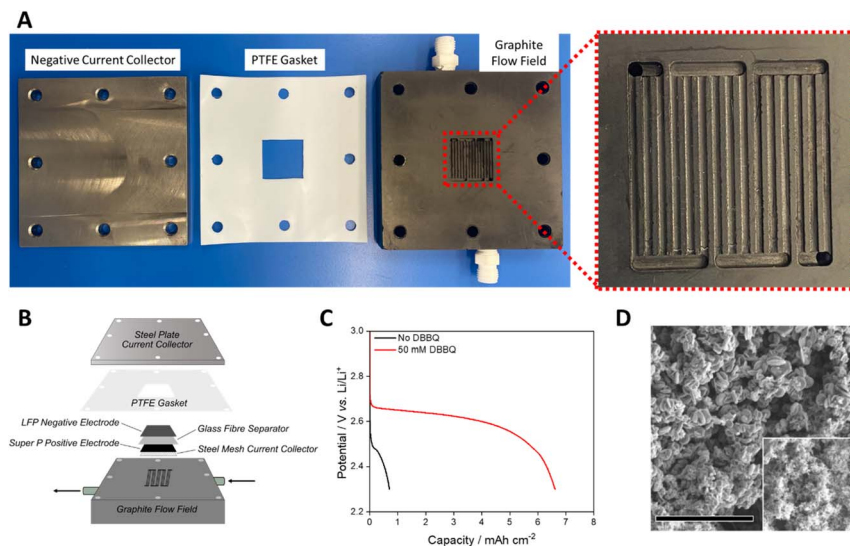
Fig. 2 (A) Photographs of the cell housing used in the study, with a magnified image of the flow field plate shown. (B) A schematic of the open Li−air cell design showing the stack composition and flow field position. (C) Discharge profiles of cells discharged under flowing 100% O_2 (0.50 mL min^{-1}) with and without the addition of 50 mM DBBQ. (D) SEM image of the positive electrode after discharge with DBBQ. The inset shows the pristine positive electrode. The scale bar is 20 μm long. The cell was discharged at a rate of 0.1 mA cm^{-2}.

Li/Li$^+$ (Fig. 2C). Low capacities have been observed previously during analysis of ether-based Li–air cells, and have been improved by the use of redox mediators.[40] The discharge was repeated with the addition 50 mM di-*tert*-butyl dibenzoquinone (DBBQ) resulting in an areal capacity of 6.6 mA h cm^{-2}, 9.4 times greater than in the absence of the redox mediator, and among the highest areal capacities recorded for a Li–air cell.[40,41] A cell containing the same electrode components in a Swagelok cell filled with a static headspace of 100% O$_2$ gave an areal capacity of 3.5 mA h cm^{-2}, demonstrating the improvement possible by the use of flowing gas (Fig. S1†). The result also supports the need for dissolved redox mediators in the cell to reach significant capacities at high current densities, even under a high flow of pure O$_2$. As such, 50 mM DBBQ was added to all subsequent cells unless otherwise stated. Fig. 2D shows scanning electron microscopy (SEM) images of the discharge product from a DBBQ-containing cell. The appearance of toroidal structures indicates that solution-mediated Li$_2$O$_2$ formation occurred on discharge.[40,42] The Li$_2$O$_2$ yield for the DBBQ-containing cell was determined to be 82% using the method developed by Hartmann *et al.*[43] (other yield measurements can be found in Table S1†). These data confirm that the Li–air demonstrator discharge performance was consistent with coin and Swagelok cells, but that the use of flowing gas improved capacity significantly.

To evaluate the performance of the open cell architecture under various operating conditions, cells were discharged under 100% O$_2$, 20% O$_2$ and air at a range of flow rates (Fig. 3). Pure O$_2$ represents optimal performance conditions
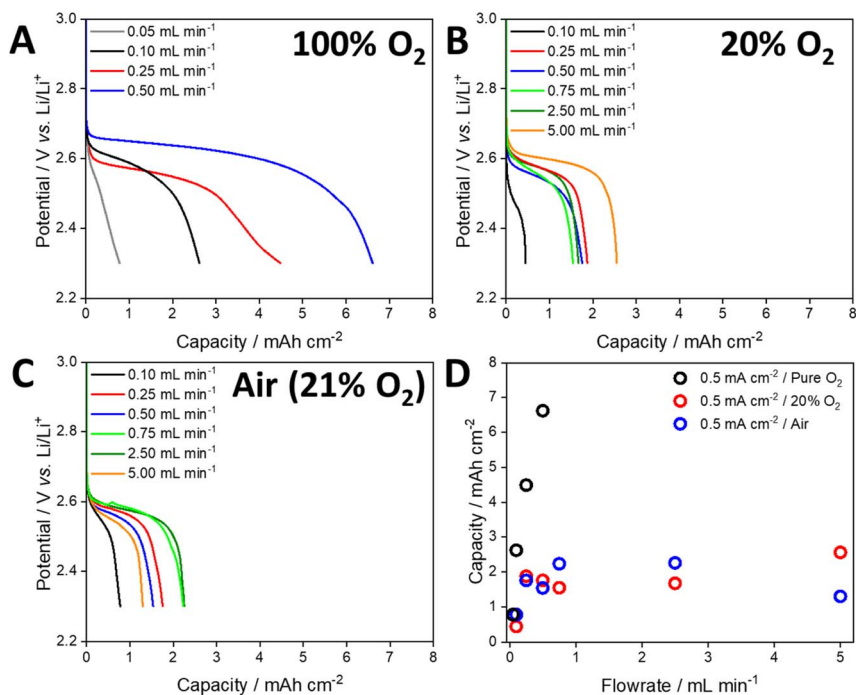

Fig. 3 Discharge profiles of cells discharged at a current density of 0.5 mA cm^{-2} under a flow of (A) 100% O$_2$, (B) 20% O$_2$ with N$_2$ balance and (C) air. (D) Shows the areal capacity of these cells.

of the open cell and matches the conditions in most studies in this field, which use a static headspace/flow of pure O_2. However, 20% O_2 better reflects the atmospheric concentration of O_2 and operation under optimum scrubber conditions (H_2O and CO_2 are completely removed). Operation under air reflects the performance in the absence of a scrubber. When using 100% O_2, the capacity of the cell was almost directly proportional to the gas flow rate (Fig. 3A). At the highest rate of 0.5 mL min^{-1}, a maximum capacity of 6.6 mA h cm^{-2} was achieved, compared to 0.8 mA h cm^{-2} at the lowest rate of 0.05 mL min^{-1}. The cell voltage (determined from the mid-point of the discharge plateau, Table S2†) was also dependent on the flow rate, indicating that O_2 depletion occurred at lower flow rates, lowering the discharge potential. When using 20% O_2 and a current density of 0.5 mA cm^{-2}, the capacity initially increased with increasing flow rate (Fig. 3B). However, beyond 0.75 mL min^{-1} the capacity did not increase, and some cells displayed a lower capacity. As expected, the discharge plateaus were lower than those observed under flows of pure O_2. Despite the use of flow rates an order of magnitude higher than those used with pure O_2, the maximum capacity that could be achieved was approximately 2.6 mA h cm^{-2}. Discharging using air gave a similar trend to that obtained using 20% O_2 (Fig. 3C and D).

Based on a 2e$^-$ reduction of O_2 and the applied current density, the rate of O_2 consumption was calculated and used to develop plots of normalised flow rate *versus* capacity (Fig. 4A, see the ESI and Table S3† for details of the calculations). When using pure O_2 and a current density of 0.5 mA cm^{-2}, the maximum capacity (6.6 mA h cm^{-2}) was achieved with a flow rate that was 33 times higher than the theoretical rate of O_2 consumption. In contrast, applying a flow rate factor of 3.3 gave an areal capacity of 0.8 mA h cm^{-2} (Fig. 4A). Despite the use of 100% O_2, this demonstrates that significant excess gas flow may be required at the positive electrode. For a flow rate factor of 33 using 20% O_2, the capacity of the cell decreased to 1.8 mA h cm^{-2} at a current density of 0.5 mA cm^{-2} (Fig. 4A). This capacity could not be significantly increased (2.6 mA h cm^{-2}) by increasing the
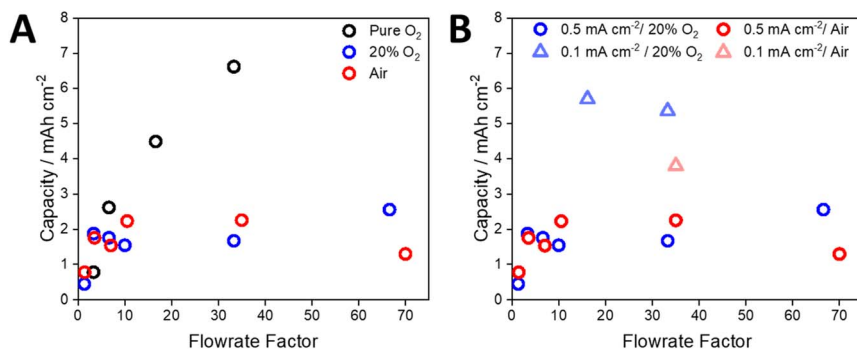
Fig. 4   (A) The capacity of the cells discharged with a current density of 0.5 mA cm^{-2} as a function of the flow rate factor, where a flow rate factor of 1 is equivalent to the rate of oxygen consumption within the cell based on the applied current density. (B) The effect of current density on the capacity of the cell when discharged under a flow of 20% O_2 and air, as a function of flow rate factor (note that data points for the 0.1 mA cm^{-2} data set correspond to absolute flow rates of 0.25 and 0.50 mL min^{-1} respectively).

flow rate factor up to 66. By reducing the applied current density to 0.1 mA cm^{-2} the cell using 20% O_2 was able to achieve a capacity similar to that using 100% O_2 (5.7 mA h) at the same flow rate factor (Fig. 4B), while noting that the absolute flow rates were different due to different gas compositions and applied current densities. These data suggest that the rate of O_2 dissolution and transport within the electrolyte solution limits the capacity of the cell under open conditions, which is particularly significant for atmospheric O_2 concentrations. While increasing the flow rate increased the capacity, very high flow rates had the opposite effect. Post-cycling analysis of the cell suggested that this was due to loss of electrolyte solution from the air electrode, which has been observed previously,[37,38] reconfirming the need for a solvent-management system.[34]

To explore the challenge of removing CO_2 and H_2O from the gas stream of an open-architecture cell, we tested the scrubber filled with either activated charcoal or molecular sieves using a flow rate factor of 35.7. Both were activated within the device by holding them at 10^{-4} mbar at 120 °C for 72 hours, approximating the conditions expected in a real Li–air gas handling system. A stream of air with relative humidity of 35% at 20 °C was used for all tests. When passing this gas composition through the scrubbing media at 20 °C, the relative humidity was almost unchanged, dropping by *ca.* 2% and 4% for activated charcoal and molecular sieves, respectively. In contrast, CO_2 levels dropped by *ca.* 32% and 41% for activated charcoal and molecular sieves, respectively (Fig. 5A). It is important to note that the volume of the scrubber far exceeded that of the headspace of the cell, indicating the need for significant innovation in scrubbing media/architecture, but the removal of significant amounts of CO_2 is promising nevertheless. Cells were discharged at 0.1 mA cm^{-2} (Fig. 5B) with and without the molecular-sieve scrubber (selected due to its ability to remove more CO_2) and the discharged cathodes were analysed by Fourier transform infra-red (FTIR) spectroscopy. In both cases, notable carbonate peaks were observed, and the intensities were similar, regardless of the lower incoming CO_2 concentration, but were much greater than that seen when using a cell discharged with 100% O_2 (Fig. 5C). The similar carbonate peak intensities, despite the drop in the gas stream CO_2 concentration, indicates a non-linear relationship between CO_2 and Li_2CO_3 formation, suggesting that near-absolute removal of CO_2 will be required for open Li–air devices.
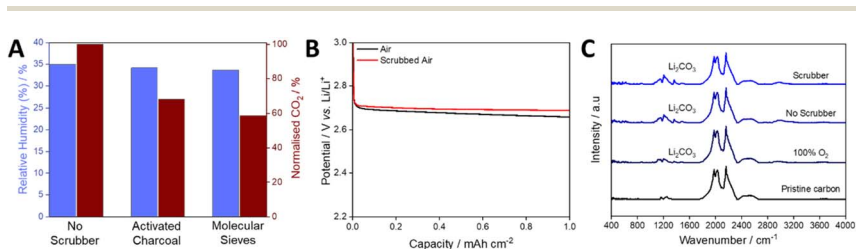
Fig. 5 (A) Relative humidity and normalised CO_2 levels of compressed air at 35% RH passed through the scrubber in the demonstrator system. (B) Discharge profiles of cells discharged in air and air that has been scrubbed using molecular sieves at 0.5 mL min^{-1} (flow rate factor 35.7) and at 0.1 mA cm^{-2}. (C) FTIR spectra of the cathodes extracted from cells discharged in 100% O_2, air and scrubbed air. Cells were discharged at a current density of 0.1 mA cm^{-2} to 5 mA h at a gas flow of 0.5 mL min^{-1}.

Faraday Discussions

Implications for the Li–air system

These data demonstrate that moving from a static head space to an open system with gas flow could offer significant increases in capacity and rate. However, when using flow fields designed for aqueous systems, the quantity of gas (O_2 or air) to be compressed, scrubbed and supplied may be significantly higher than the volume theoretically required by the cell,[44] and the higher flow rates required can lead to cell drying by evaporating the solvent. This will increase the need for saturation and capture of solvent from the gas stream.[37,38,45] For Li–air to become a commercially viable battery technology, we anticipate the need for a system-specific energy of >400 W h kg^{-1}.[3,33] Our calculations suggest that if a positive electrode capable of storing 40% vol. Li_2O_2 (approximately 30 mA h cm^{-2}) can be achieved, then a system-level energy density of an "open" architecture Li–air cell could reach >450 W h kg^{-1} (see Table S4†). Achieving this target will require the development of better gas diffusion electrodes and flow fields for electrodes, as well as organic solvents that can sustain O_2 delivery to the cell at low flow rates.

Considering the gas scrubber, neither molecular sieves nor activated carbon was able to scrub H_2O and CO_2 from the gas stream, despite the scrubber being significantly larger than the cell. This highlights the need for further innovation in the development of scrubber materials or membranes to selectively allow O_2 transport. We note that improvements in the efficiency of gas delivery to the electrode could lessen the burden on the scrubber and that the removal of CO_2 was better than that of H_2O, potentially simplifying its removal. An alternative approach is to redesign the cell chemistry to tolerate both H_2O and CO_2.[46,47] It is known that H_2O can be tolerated at greater levels than originally thought, and can even be beneficial.[42,48] Some progress has also been made in understanding the impact of LiOH and Li_2CO_3 within metal–air cells,[35,49–51] but further optimisation is required for operation in air.

Conclusion

Here we have described an integrated Li–air battery with in-line gas handling system that achieves areal capacities of *ca.* 7 mA h cm^{-2} at 0.5 mA cm^{-2} when using redox mediators. The capacity of the cell is directly proportional to the gas flow when using pure O_2, but the volume of gas required by the cell during discharge far outweighs the theoretical gas consumption at the positive electrode. This phenomenon is exacerbated in air due to its lower O_2 concentration and may be due to the use of flow-field plates designed for aqueous systems. No scrubber material tested in this study successfully removed H_2O and CO_2 from the gas stream, but a marked decrease in CO_2 concentration was observed. These data highlight the challenges that must be overcome if we are to achieve a practical air-breathing Li–air battery, including the need for better flow field plates, gas diffusion electrodes that can support 30 mA h cm^{-2} at lower flow rates, and new gas-scrubbing materials to more efficiently remove H_2O and CO_2. Critically, advances in one area will lower the requirements elsewhere. For example, improved gas delivery to the cell will reduce the volume of gas required and put less pressure on the performance of the scrubber. Alternatively, improving the cell's tolerance to H_2O and CO_2 will similarly lessen, or even remove, reliance on the gas scrubber entirely.

Author contributions

All authors contributed to the conception and design of the study. JWJ, GV, CH, MJ, RCM, and CP performed the experiments. All authors contributed to manuscript writing. BT, AL, XG, DAW, GNN, PGB and LRJ supervised the project.

Conflicts of interest

There are no conflicts to declare.

Acknowledgements

References

1 W.-J. Kwak, Rosy, D. Sharon, C. Xia, H. Kim, L. R. Johnson, P. G. Bruce, L. F. Nazar, Y.-K. Sun, A. A. Frimer, M. Noked, S. A. Freunberger and D. Aurbach, *Chem. Rev.*, 2020, **120**, 6626–6683.

2 A. Manthiram and L. Li, *Adv. Energy Mater.*, 2015, **5**, 1401302.

3 D. Aurbach, B. D. McCloskey, L. F. Nazar and P. G. Bruce, *Nat. Energy*, 2016, **1**, 16128.

4 J.-H. Kang, J. Lee, J.-W. Jung, J. Park, T. Jang, H.-S. Kim, J.-S. Nam, H. Lim, K. R. Yoon, W.-H. Ryu, I.-D. Kim and H. R. Byon, *ACS Nano*, 2020, **14**, 14549–14578.

5 L. Ma, T. Yu, E. Tzoganakis, K. Amine, T. Wu, Z. Chen and J. Lu, *Adv. Energy Mater.*, 2018, **8**, 1800348.

6 D. Kundu, R. Black, B. Adams and L. F. Nazar, *ACS Cent. Sci.*, 2015, **1**, 510–515.

7 F. Li, T. Zhang and H. Zhou, *Energy Environ. Sci.*, 2013, **6**, 1125–1141.

8 S. A. Freunberger, Y. Chen, Z. Peng, J. M. Griffin, L. J. Hardwick, F. Barde, P. Novak and P. G. Bruce, *J. Am. Chem. Soc.*, 2011, **133**, 8040–8047.

9 D. Sharon, M. Afri, M. Noked, A. Garsuch, A. A. Frimer and D. Aurbach, *J. Phys. Chem. Lett.*, 2013, **4**, 3115–3119.

10 B. D. McCloskey, A. Valery, A. C. Luntz, S. R. Gowda, G. M. Wallraff, J. M. Garcia, T. Mori and L. E. Krupp, *J. Phys. Chem. Lett.*, 2013, **4**, 2989–2993.

11 R. C. McNulty, K. Jones, C. Holc, J. W. Jordan, P. G. Bruce, D. A. Walsh, G. N. Newton, H. W. Lam and L. R. Johnson, *Adv. Energy Mater.*, 2023, **13**, 2300579.

12 N. Mozhzhukhina, F. Marchini, W. R. Torres, A. Y. Tesio, L. P. Mendez De Leo, F. J. Williams and E. J. Calvo, *Electrochem. Commun.*, 2017, **80**, 16–19.

13 L. Johnson, C. Li, Z. Liu, Y. Chen, S. A. Freunberger, P. C. Ashok, B. B. Praveen, K. Dholakia, J. M. Tarascon and P. G. Bruce, *Nat. Chem.*, 2014, **6**, 1091–1099.

14 J. Højberg, B. D. McCloskey, J. Hjelm, T. Vegge, K. Johansen, P. Norby and A. C. Luntz, *ACS Appl. Mater. Interfaces*, 2015, **7**, 4039–4047.

15 V. Viswanathan, K. S. Thygesen, J. S. Hummelshoj, J. K. Norskov, G. Girishkumar, B. D. McCloskey and A. C. Luntz, *J. Chem. Phys.*, 2011, **135**, 214704.

16 S. Ahn, C. Zor, S. Yang, M. Lagnoni, D. Dewar, T. Nimmo, C. Chau, M. Jenkins, A. J. Kibler, A. Pateman, G. J. Rees, X. Gao, P. Adamson, N. Grobert, A. Bertei, L. R. Johnson and P. G. Bruce, *Nat. Chem.*, 2023, **15**, 1022–1029.

17 Y. Chen, S. A. Freunberger, Z. Peng, O. Fontaine and P. G. Bruce, *Nat. Chem.*, 2013, **5**, 489–494.

18 B. J. Bergner, A. Schurmann, K. Peppler, A. Garsuch and J. Janek, *J. Am. Chem. Soc.*, 2014, **136**, 15054–15064.

19 N. Feng, X. Mu, X. Zhang, P. He and H. Zhou, *ACS Appl. Mater. Interfaces*, 2017, **9**, 3733–3739.

20 Y. Chen, X. Gao, L. R. Johnson and P. G. Bruce, *Nat. Commun.*, 2018, **9**, 767.

21 H.-D. Lim, B. Lee, Y. Zheng, J. Hong, J. Kim, H. Gwon, Y. Ko, M. Lee, K. Cho and K. Kang, *Nat. Energy*, 2016, **1**, 16066.

22 V. Pande and V. Viswanathan, *ACS Energy Lett.*, 2017, **2**, 60–63.

23 Q. C. Liu, J. J. Xu, S. Yuan, Z. W. Chang, D. Xu, Y. B. Yin, L. Li, H. X. Zhong, Y. S. Jiang, J. M. Yan and X. B. Zhang, *Adv. Mater.*, 2015, **27**, 5241–5247.

24 X. Bi, K. Amine and J. Lu, *J. Mater. Chem. A*, 2020, **8**, 3563–3573.

25 S. Matsuda, M. Ono, S. Yamaguchi and K. Uosaki, *Mater. Horiz.*, 2022, **9**, 856–863.

26 Y. Kubo and K. Ito, *ECS Trans.*, 2014, **62**, 129–135.

27 S. Zhao, L. Zhang, G. Zhang, H. Sun, J. Yang and S. Lu, *J. Energy Chem.*, 2020, **45**, 74–82.

28 H. C. Lee, J. O. Park, M. Kim, H. J. Kwon, J.-H. Kim, K. H. Choi, K. Kim and D. Im, *Joule*, 2019, **3**, 542–556.

29 J. O. Park, M. Kim, J.-H. Kim, K. H. Choi, H. C. Lee, W. Choi, S. B. Ma and D. Im, *J. Power Sources*, 2019, **419**, 112–118.

30 T. Zhang and H. Zhou, *Nat. Commun.*, 2013, **4**, 1817.

31 D. Cao, C. Tan and Y. Chen, *Nat. Commun.*, 2022, **13**, 4908.

32 Z. Zhao, J. Huang and Z. Peng, *Angew. Chem., Int. Ed.*, 2018, **57**, 3874–3886.

33 A. C. Luntz and B. D. McCloskey, *Chem. Rev.*, 2014, **114**, 11721–11750.

34 K. G. Gallagher, S. Goebel, T. Greszler, M. Mathias, W. Oelerich, D. Eroglu and V. Srinivasan, *Energy Environ. Sci.*, 2014, **7**, 1555–1563.

35 M. Asadi, B. Sayahpour, P. Abbasi, A. T. Ngo, K. Karis, J. R. Jokisaari, C. Liu, B. Narayanan, M. Gerard, P. Yasaei, X. Hu, A. Mukherjee, K. C. Lau, R. S. Assary, F. Khalili-Araghi, R. F. Klie, L. A. Curtiss and A. Salehi-Khojin, *Nature*, 2018, **555**, 502–506.

36 H. J. Kwon, H. C. Lee, J. Ko, I. S. Jung, H. C. Lee, H. Lee, M. Kim, D. J. Lee, H. Kim, T. Y. Kim and D. Im, *J. Power Sources*, 2017, **364**, 280–287.

37 J. P. O. Júlio, B. A. B. Francisco, B. P. de Sousa, J. F. Leal Silva, C. G. Anchieta, T. C. M. Nepel, C. B. Rodella, R. Maciel Filho and G. Doubek, *Chem. Eng. J. Adv.*, 2022, **10**, 100271.

38 B. A. B. Francisco, J. P. O. Júlio, C. G. Anchieta, T. C. M. Nepel, R. M. Filho and G. Doubek, *ACS Appl. Energy Mater.*, 2023, **6**, 5167–5176.

39 M. Sauermoser, N. Kizilova, B. G. Pollet and S. Kjelstrup, *Front. Energy Res.*, 2020, **8**, 1–20.

40 X. Gao, Y. Chen, L. Johnson and P. G. Bruce, *Nat. Mater.*, 2016, **15**, 882–888.

41 X. Gao, Y. Chen, L. R. Johnson, Z. P. Jovanov and P. G. Bruce, *Nat. Energy*, 2017, **2**, 17118.

42 N. B. Aetukuri, B. D. McCloskey, J. M. García, L. E. Krupp, V. Viswanathan and A. C. Luntz, *Nat. Chem.*, 2015, **7**, 50–56.

43 P. Hartmann, C. L. Bender, J. Sann, A. K. Dürr, M. Jansen, J. Janek and P. Adelhelm, *Phys. Chem. Chem. Phys.*, 2013, **15**, 11661–11672.

44 L. Grande, E. Paillard, J. Hassoun, J. B. Park, Y. J. Lee, Y. K. Sun, S. Passerini and B. Scrosati, *Adv. Mater.*, 2015, **27**, 784–800.

45 F. Mohazabrad, F. Wang and X. Li, *ACS Appl. Mater. Interfaces*, 2017, **9**, 15459–15469.

46 H. A. Gasteiger, M. Piana, T. Restle, M. Metzger and K. U. Schwenke, *J. Electrochem. Soc.*, 2015, **162**, A573–A584.

47 D. G. Kwabi, T. P. Batcho, S. Feng, L. Giordano, C. V. Thompson and Y. Shao-Horn, *Phys. Chem. Chem. Phys.*, 2016, **18**, 24944–24953.

48 M. C. Policano, C. G. Anchieta, T. C. M. Nepel, R. M. Filho and G. Doubek, *ACS Appl. Energy Mater.*, 2022, **5**, 9228–9240.

49 S. Ko, Y. Yoo, J. Choi, H.-D. Lim, C. B. Park and M. Lee, *J. Mater. Chem. A*, 2022, **10**, 20464–20472.

50 Z. Gao, I. Temprano, J. Lei, L. Tang, J. Li, C. P. Grey and T. Liu, *Adv. Mater.*, 2023, **35**, 2201384.

51 H. Wakita, R. Awata, Y. Maita and T. Takeguchi, *J. Phys. Chem. C*, 2023, **127**, 10012–10024.